P2.8 TOTAL LIGHTNING FREQUENCY IN RELATION TO ICE MASSES AND ICE MASS FLUX ESTIMATES

W. Deierling *[1] , W. A. Petersen [2] , J. Latham [3] , S. M. Ellis [3], H. J. Christian Jr. [4] and J. Walters[1]

[1] University of Alabama, Huntsville, Alabama
[2] Earth System Science Center, University of Alabama, Huntsville, Alabama
[3] National Center for Atmospheric Research, Boulder, Colorado
[4] Global Hydrology & Climate Center, NSSTC, Huntsville, Alabama

1. INTRODUCTION

In general a strong updraft in the mixed phase region is needed to produce lightning. This is the region where the non-inductive charging mechanism (Reynolds et al., 1957; Takahashi, 1978; Saunders et al., 1991; Saunders 1993) is generally believed to generate most of the thunderstorm electrification. This mechanism involves rebounding collisions between graupel and ice crystals in the presence of supercooled liquid water. The charge transfer per collision depends on size of the ice crystals and the fall-speed of the graupel pellets, while the sign of the charging depends on temperature and the liquid water content. Significant charging occurs where graupel, ice crystals and supercooled droplets co-exist. This region is referred to as the charging zone. Its vertical extent is limited (Latham et al., 2004), and its boundaries are somewhat diffuse. The upper limit is usually the level above which graupel can no longer be supported by the updraft, typically between the -15°C and -30°C isotherms, and therefore increases with increasing updraft speed, w. Most of the charging that is crucial to lightning production occurs just beneath this upper limit height, principally because the charge transfer per collision increases rapidly with crystal size. The level of the lower boundary is dependent upon the prevailing glaciation mechanism, but can characteristically be taken as a few degrees colder than 0°C.

Based on these ideas, analytical calculations by Blyth et al. (2001), Latham et al. (2004) and Petersen and Rutledge (2001) yielded the prediction that the lightning frequency f was roughly proportional to the product of the downward flux p of solid precipitation (graupel) and the upward mass-flux I of ice crystals, the values of p and I being those existing at the top of the charging zone. Hereafter this will be referred to as the flux hypothesis. The predicted equation valid in the charging zone that describes the flux hypothesis is:

$$f = C \cdot p \cdot I,$$

where C is a constant.

Support for the flux hypothesis was provided by computations made with multiple lightning activity models by Baker et al. (1995) and Baker et al. (1999). These initial investigations show promising results for the predicted relationship between total lighting activity and the product of the upward ice flux and the downward precipitation ice flux. Nevertheless, the predicted relationship is currently lacking more definite support from field data.

In this study the relationship of total lightning activity as a function of precipitation and non precipitation ice mass as well as estimates of their fluxes will be investigated. To examine particle interactions in the turbulent mixed phase regions of thunderstorms, polarimetric radar data was used to identify bulk microphysical hydrometeor types (Straka et al. 2000; Vivekanandan et al. 1999), and mass contents of various particles (Straka et al. 2000). It has to be kept in mind that radar measurements are dominated by the largest particles in a given radar volume thus smaller ice crystals in the charging zone will go undetected. To compute flux estimates, three dimensional wind fields were calculated from dual Doppler radar data. In one case radar data from only one radar was available. Here a three dimensional wind field was determined using the National Center for Atmospheric Science's (NCAR's) Variational Doppler Radar Assimilation System (VDRAS) (Sun and Crook, 1997; Sun and Crook, 2001; Crook and Sun, 2004).

This study uses data from 7 different thunderstorms, which are of different type and originated in two different climate regions of the United States: the High Plains and Northern Alabama. Data from these storms are from the Severe Thunderstorm Electrification and Precipitation Study (STEPS) project which took place at the Colorado/Kansas border in the summer of 2000, from the Stratospheric-Tropospheric Experiment: Radiation, Aerosols and Ozone (STERAO)

*Corresponding author address: Wiebke Deierling, Univ. Ala. Huntsville, Dept. Atmos. Science, 320 Sparkman Dr., Huntsville Al., 35805; email: deierling@nsstc.uah.edu

experiment that took place in the summer of 1996 in Northern Colorado and from Northern Alabama where the University of Alabama Huntsville/National Space Science and Technology Center (UAH/NSSTC) ARMOR radar (Petersen et al. 2005) was used with a nearby WSR-88D (Weather Surveillance Radar-1988 Doppler) radar which allows dual Doppler synthesis to be performed under the coverage umbrella of the N. Alabama lightning mapping array (LMA). These data were used to study the lifecycle of a storm that produced small hail on April 7 2005. During STERAO polarimetric radar data were collected from the Colorado State University (CSU)-CHILL radar and total lightning activity was recorded by the Office Nationale d'Etudes et de Recherches Aerospatiales (ONERA) 3-D lightning interferometer as well as cloud-to-ground lightning by the National Lightning Detection Network (NLDN). These data were used to study the lifecycle of a severe storm observed on 10 July 1996 that exhibited multicellular and later in its lifetime supercellular character. During STEPS, polarimetric radar data were collected from the CSU-CHILL radar as well as from the National Center for Atmospheric Research S-band dual-polarimetric Doppler weather radar (S-POL). Total lighting activity was recorded by the New Mexico Institute of Mining and Technology (NMIMT) deployable Lightning Mapping System (LMS) and cloud-to-ground lightning data were available from NLDN. In this study several storms that were observed on June 6 and July 5 2000 were analyzed. These storms included "garden variety storms", a tornadic supercell as well as a splitting supercell with a subsequent left and right mover.

2. METHOD

First, to determine bulk hydrometeor types within thunderstorms from polarimetric radar data, the NCAR particle identification algorithm (PID) (Vivekanandan 1999) was applied. It determines bulk hydrometeor types in radar space and is based on a fuzzy logic algorithm which uses nine input variables: the radar reflectivity, the differential reflectivity, the linear depolarization ratio, the correlation coefficient, the specific differential phase, a temperature profile, the standard deviation of velocity, the standard deviation of differential reflectivity and the standard deviation of the differential phase to distinguish between 17 output categories. Those are: cloud droplets, drizzle, light rain, moderate rain, heavy rain, hail, hail/rain mix, graupel/small hail, graupel/small hail/rain mix, dry snow, wet snow, irregular ice crystals, horizontal oriented ice crystals, super cooled liquid drops, insects, second trip, and ground clutter. It can be seen that 14 of these categories are hydrometeor related. To relate the microphysics data to a 3D wind field on a Cartesian grid the PID output, temperature and reflectiviy was gridded with the NCAR/EOL software package REORDER using a closest point weighting scheme. Due to microphysical reasons as well as similarities between hydrometeor classifications, two or more particle types were in some cases added together. In this study the hail, hail/rain mix, graupel/small hail and graupel/small hail/rain mix PID categories above the height of the -5°C level were taken to represent precipitation ice in the charging zone over individual radar volumes. As mentioned in the introduction, ice crystals are not detected in the updraft region by the radar. Therefore as a rough estimate, PID-identified dry snow, irregular ice and oriented ice crystal categories above the -45°C level and with reflectivity values below 20 dBZ were chosen to represent non precipitation ice. As another estimate for non precipitation ice these categories colder than -35°C and with a divergence larger than 0.001 s^{-1} and reflectivity values below 20 dBZ were chosen as a proxy for non precipitation ice mass from the charging zone. Using the divergence to identify non precipitation ice coming from the updraft originates from the assumption that the continuity equation is satisfied in the anelastic form:

$$\nabla_H \rho_0 V = \partial (w \rho_0) \setminus \partial z ,$$

where ρ_0 is the base state density (as stated above a function of height only), w is the vertical velocity and V is the horizontal velocity. One can see that the horizontal mass divergence (left side) is equal to the change of vertical mass flux with height (right side), assuming also that w = 0 m/s at the top of the thunderstorm and at the surface. Thus at a given level, an increase in w with height is expected to be accompanied by horizontal convergence, a decrease in w with height by horizontal divergence. This leads to the assumption of low level mass convergence below the maximum in w and upper level mass divergence above the maximum in w (e.g. Witt and Nelson, 1991; Yuter and Houze, 1995). The assumption here is that the upper level horizontal divergence above a threshold can be used to approximate non precipitation ice out of the updraft. The divergence was calculated using the dual Doppler synthesis or VDRAS.

Precipitation ice and non precipitation ice mass contents were computed using reflectivity (Z) – mass content (M) relationships of the kind $M = aZ^b$ from the literature that appear to represent adequately different thunderstorm ice types. Note that mass contents using various relationships for an individual particle type were compared and it was found that though values varied in magnitude, computed total mass trends were not modified greatly. The Z-M relationships used for hail, graupel and thunderstorm anvil ice are given in Table 1. The reflectivity factor Z is multiplied by a factor of 5.28 (Sassen, 1987) to account for the lower dielectric constant for ice.

Hydro-meteor categories	NCAR PID categories	Z-M relation-ship [g/m^3]	Reference
Non precip ice	Dry snow, Oriented ice, Irregular ice	M = 0.017 * $Z^{0.529}$	Heymsfield and Palmer, 1986
Graupel	Graupel, Graupel/rain mixture	M = 0.0052 * $Z^{0.5}$	Heymsfield and Miller, 1988
Hail	Hail, Hail/rain mixture	M = 0.000044 * $Z^{0.71}$	Heymsfield and Miller, 1988

Table 1. M-Z relationships for various hydrometeor types .

For each of the PID categories listed in Table 1, ice mass contents for individual grid points were calculated, multiplied by their volume and then summed over the radar volume. The center time of a volume scan was addressed to the volume.

During STEPS the S-Pol and CHILL radars were positioned to allow dual Doppler synthesis. For the Huntsville, Alabama area, the ARMOR radar together with the Hytop WSR-88D radar allow dual Doppler synthesis and for STERAO, VDRAS was used to determine horizontal divergence and three dimensional wind fields. For the dual Doppler synthesis, first radar velocities were unfolded manually using the NCAR software soloii. Contamination such as second trip and ground clutter were removed using the PID information.

For the C-band ARMOR radar, the reflectivity and the differential reflectivity were corrected for attenuation and specific attenuation respectively using locally modified software from the BMRC C-pol radar (developed by V.N. Bringi at CSU and shared by T. Keenan, BMRC) that uses a FIR/adaptive spatial filter approach to compute differential and specific differential phase. Second, the NCAR Reorder software was used to interpolate the radar data from radar space onto a Cartesian grid. A Cressman filter weighting function was used for the conversion. Finally the NCAR Custom Editing and Display of Reduced Information in Cartesian Space (CEDRIC) software was used to determine a three dimensional wind field (u,v as the horizontal wind components and w as the vertical wind component). Vertical wind velocities were determined with three separate methods: integrating the mass continuity equation upward, downward and variationally. The calculations take the hydrometeor terminal fall speeds into account. Thus vertical velocities w were determined as the difference between the measured vertical velocities W from the solution of the mass continuity equation and a bulk estimate of the fall speed of precipitation particles v_t: w = W- v_t (Rogers and Tripp, 1964).

As a flux proxy of the product of non precipitation ice mass flux and precipitation ice mass flux, the product of precipitation ice mass above the -5°C level and vertical wind speeds larger than 0 m/s was multiplied with non precipitation ice that was situated colder than -35°C, at a divergence larger than 0.001 s^{-1} and reflectivity values below 20 dBZ.

3. RESULTS

Total precipitation, non precipitation ice mass and flux proxy totals of individual radar volumes were compared to the total, smoothed total (with a running boxcar average of the radar volume time) and mean total lightning activity during the radar volume time. Several lightning 'parameters' were calculated because the lightning measurement is continuous in time and space whereas the radar measurement is not. Results from 7 storms including garden variety storms, storms of multicellular and supercellular character are presented.

3.1 CORRELATION BETWEEN PRECIPITATION ICE MASS AND TOTAL LIGHTNING

Total amounts of precipitation ice mass above the -5°C level per radar volume were plotted against the total, the smoothed total and mean lighting amounts per radar volume. The correlation between total, smoothed total and mean lightning amounts and total precipitation

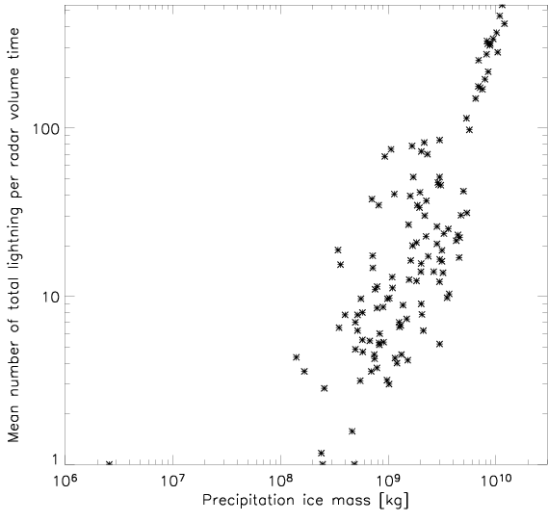

Figure 1. Precipitation ice mass above the -5°C level versus mean total lightning per radar volume time on a logarithmic scale.

ice mass per radar volume time is high with correlation coefficients of 0.87, 0.88 and 0.9 respectively. Figure 1 shows the scatter plot for precipitation ice mass versus the mean number of total lighting per radar volume time of all 7 storms investigated.

3.2 CORRELATION BETWEEN NON PRECIPITATION ICE MASS AND TOTAL LIGHTNING

First, totals of non precipitation ice mass above the -45°C level and with reflectivity values smaller than 20 dBZ per radar volume were plotted against the total, the smoothed total and mean lighting amounts per radar volume. Here the correlation between total, smoothed total and mean lightning amounts and total non precipitation ice mass per radar volume time is lower than for those of the precipitation ice mass. Correlation coefficients are 0.76, 0.77 and 0.78 respectively. Figure 2 shows the scatter plot for non precipitation ice mass above the -45°C level, with reflectivity values smaller than 20 dBZ versus the mean number of total lighting per radar volume time for all 7 storms again.

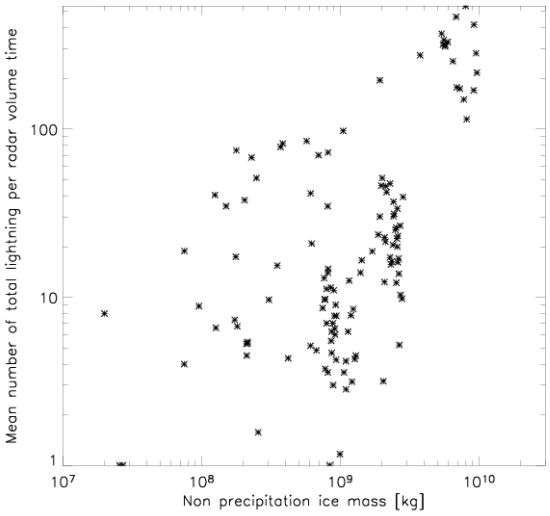

Figure 2. Non precipitation ice mass above the -45°C level and with reflectivity values smaller than 20 dBZ versus mean total lightning per radar volume time on a logarithmic scale.

Second, totals of non precipitation ice mass above the -35°C level, reflectivity values smaller than 20 dBZ and divergence larger than 0.001 s^{-1} were examined. These results indicate better correlations of 0.90, 0.91 and 0.93 respectively. Figure 3 shows the mean total lightning activity per radar volume time and the corresponding non precipitation ice proxy.

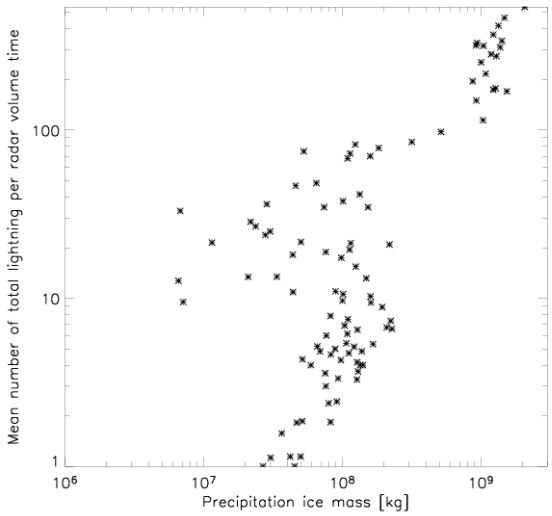

Figure 3. Non precipitation ice mass above the -35°C level, with reflectivity values smaller than 20 dBZ and divergence larger than 0.001 s^{-1} versus mean total lightning per radar volume time on a logarithmic scale.

3.3 CORRELATION BETWEEN THE FLUX PROXY AND TOTAL LIGHTNING

Finally a flux proxy for the product of non precipitation and precipitation ice mass flux was calculated. The proxy is the product of precipitation ice mass and vertical wind speeds larger than 0 m/s and colder than -5°C was multiplied with non precipitation ice colder than -35°C, a divergence larger than 0.001 s^{-1} and reflectivity values below 20 dBZ. Figure 4 shows a scatter plot of the flux proxy and mean total lightning discharges per radar volume. The correlation between the flux proxy and total, smoothed total and mean total lightning is higher than those involving just ice masses. The correlation coefficients of the flux proxy and total, smoothed total and mean total lightning per radar volume are 0.92, 0.93 and 0.95 respectively.

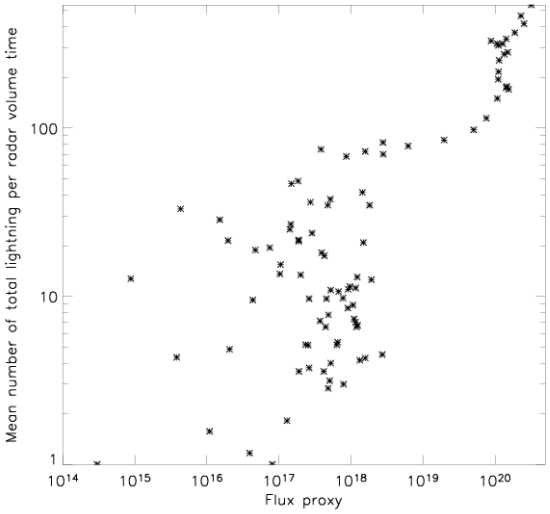

Figure 4. Flux proxy as the product of non precipitation ice mass above the -35°C level, with reflectivity values smaller than 20 dBZ, divergence greater than 0.001 s^{-1} and precipitation ice above -5°C multiplies with updraft velocities greater 0 m/s versus mean total lightning per radar volume time on a logarithmic scale.

5. CONCLUSIONS

Overall bulk microphysical trends of precipitation and non precipitation ice mass estimates show a good relationship to total lightning activity for the total of 7 storms of different types and from two different climate regions. Furthermore computing a flux estimate improves the correlation to total lightning activity, giving support for the flux hypothesis.

6. ACKNOLEDGEMENTS

WAP and WD acknowledge funding from NASA ESE Lightning Imaging Sensor Project. JL wishes to acknowledge the support of USRA/NASA. The authors gratefully acknowledge Mr. David Brunkow and Mr. Patrick Kennedy for providing the CHILL radar data, Dr. Eric Defer for providing total lightning data for the STERAO 10 July storm and Dr. Andrew Crook for providing 3D wind and divergence fields for the 10 July storm retrieved from VDRAS.

7. REFERENCES

Baker, M.B., H.J. Christian and J. Latham, 1995: A computational study of the relationships linking lightning frequency and other thundercloud parameters. Q. J. R. Meteorol. Soc., **121**, 1525-1548.

Baker, M.B., A.M. Blyth, H.J. Christian, A.M. Gadian, J. Latham and K. Miller, 1999: Relationships between lightning activity and various thundercloud parameters: satellite and modelling studies. Atmos. Res., **51**, 221-236.

Blyth, A.M., H.J. Christian, K. Driscoll, A.M. Gadian and J. Latham, 2001: Determination of ice precipitation rates and thunderstorm anvil ice contents from satellite observations of lightning. Atmos. Res., **59-60**, 217-229.

Crook, N.A. and J. Sun, 2004: Analysis and Forecasting of the Low-Level Wind during the Sydney 2000 Forecast Demonstration Project. Wea. Forecasting, **19**, 151-167.

Heymsfield, A.J., and A.G. Palmer, 1986: Relations for deriving thunderstorm anvil mass of CCOPE storm water budget estimates. J. Climate Appl. Meteor., **25**, 691-702.

Heymsfield, A.J, and K.M. Miller, 1988: Water Vapor and Ice Mass Transported into the Anvils of CCOPE Thunderstorms: Comparison with Storm Influx and Rainout. J. Atmos Sci., **45**, 3501-3514.

Latham, J. A.M. Blyth, H.J. Christian Jr., W. Deierling and A.M. Gadian, 2004: Determination of precipitation rates and yields from lightning measurements. Journal of Hydrology, **288**, 13-19.

Petersen, W.A. and S.A. Rutledge, 2001: Regional Variability in Tropical Convection: Observations from TRMM. J. Climate, **14**, 3566-3586.

Petersen, W.A., K. Knupp, J. Walters, W. Deierling, M. Gauthier, B. Dolan, J.P. Dice, D. Satterfield, C. Davis, R. Blakeslee, S. Goodman, S. Podgorny, J. Hall, M. Budge and A. Wooten: The UAH-NSSTC/WHNT ARMOR C-band dual-polarimetric radar: A unique collaboration in research, education and technology transfer. Preprints, AMS 32nd Conference on Radar Meteorology, Albuquerque, New Mexico, 24-29 October 2005.

Reynolds, S.E., M. Brook and M.F. Gourley, 1957: Thunderstorm charge separation. J. Atmos. Sci., **14**, 426-436.

Rogers, R.R and B.R. Tripp. 1964: Some Radar Measurements of Turbulence in Snow. J. Appl. Meteor., **3**, 603-610.

Sassen, K., 1987: Ice Cloud Content from Radar Reflectivity. J. of Climate and Appl. Meteor., **26**, 1050-1053.

Saunders, C.P.R., W.D. Keith and R.P. Mitzeva, 1991: The effect of liquid water on thunderstorm charging. J. Geophys. Res., **96**, 11007-11017.

Saunders , C. P. R., 1993 : A Review of Thunderstorm Electrification Processes. J. Appl. Meteor., **32**, 642-655.

Straka J.M., D.S. Zrnic, A.V. Ryshkov, 2000: Bulk hydrometeor classification and quantification using polarimetric radar data: synthesis of relations. J. Appl. Meteor.,**39**, 1341-1372.

Sun,J. and N. A. Crook, 1997: Dynamical and Microphysical Retrieval from Doppler Radar Observations Using a Cloud Model and Its Adjoint. Part I: Model Development and Simulated Data Experiments. J. Atmos. Sci., **55**, 835-852.

Sun,J. and N. A. Crook, 2001: Real-Time Low-Level Wind and Temperature Analysis Using Single WSR-88D Data. Wea. Forecasting, **16**, 117-132.

Takahashi, T., 1978: Riming electrification as a charge generation mechanism in thunderstorms. J. Atmos. Sci., **35**, 1536-1548.

Vivekanandan, J., D.S. Zrnic, S. M. Ellis, R. Oye, A. V. Ryzhkov, and J. Straka, 1999: Cloud microphysics retrieval using S-band dual-polarization radar measurements. Bull. Amer. Meteor. Soc., **80**, 381-388.

Witt. A. and S.P. Nelson, 1991: The Use of Single Doppler Radar for Estimating Maximum Hailstone Size. J. Appl. Meteor., **30**, 425-431.

Yuter, S.E. and R.A. Houze Jr., 1995, Three-Dimensional Kinematic and Microphysical Evolution of Florida Cumulonimbus. Part III: Vertical Mass Transport, Mass Divergence, and Synthesis. Mon. Wea. Rev., **123**, 1964-183.